Journal of Microscopy, Vol. 199, Pt 1, July 2000, pp. 79–84.
Received 9 November 1998; accepted 18 February 2000

Using the Hilbert transform for 3D visualization of differential interference contrast microscope images

M. R. ARNISON*, C. J. COGSWELL*†, N. I. SMITH*, P. W. FEKETE* & K. G. LARKIN*
**Department of Physical Optics, School of Physics, University of Sydney, NSW, 2006, Australia*
†Australian Key Centre for Microscopy and Microanalysis, University of Sydney, NSW, 2006, Australia

Key words. 3D microscopy, 3D visualization, chromosome, confocal microscopy, DIC, differential interference contrast, Hilbert transform, image processing.

Summary

Differential interference contrast (DIC) is frequently used in conventional 2D biological microscopy. Our recent investigations into producing a 3D DIC microscope (in both conventional and confocal modes) have uncovered a fundamental difficulty: namely that the phase gradient images of DIC microscopy cannot be visualized using standard digital image processing and reconstruction techniques, as commonly used elsewhere in microscopy. We discuss two approaches to the problem of preparing gradient images for 3D visualization: integration and the Hilbert transform. After applying the Hilbert transform, the dataset can then be visualized in 3D using standard techniques. We find that the Hilbert transform provides a rapid qualitative pre-processing technique for 3D visualization for a wide range of biological specimens in DIC microscopy, including chromosomes, which we use in this study.

Introduction

Biomedical researchers are increasing their use of 3D visualization in examining the behaviour of small structures such as the cytoskeleton and chromosomes during mitosis. Much of this work is carried out using fluorescence, especially confocal fluorescence, which is ideally suited to 3D analysis (Terasaki & Dailey, 1995; Hepler & Gunning, 1998). However, there is a continuing need to observe unstained transparent features within biological specimens, accounting for the continuing popularity of differential interference contrast (DIC) in conventional microscopes (Cole *et al.*, 1995). The use of DIC is currently limited to 2D, as attention has only recently been paid to 3D visualization for transmission DIC. This contrasts with the advanced development of 3D visualization techniques for fluorescence.

Correspondence: Matthew R. Arnison, School of Physics A28, University of Sydney NSW 2006, Australia. Tel: + 612 9351 6874; fax: + 612 9351 7727; e-mail: mra@physics.usyd.edu.au.

We are investigating 3D DIC microscopy, in both conventional and confocal modes. We have found that standard 3D image processing and visualization techniques, such as those used for confocal fluorescence, are inappropriate for DIC.

DIC produces an image combining the phase gradient and amplitude of the specimen. For weakly absorbing objects, the image will be mostly phase information. This provides structural information about otherwise transparent details of the specimen, where there are changes in refractive index in features such as cell components. The response to the phase-gradient is non-linear, so without correction to a linear response, any resulting 3D visualization will be qualitative only, just as for the original 2D DIC images. In this paper we concentrate on such qualitative imaging.

A simulated 1D cross-section of a phase object and its DIC phase gradient is shown in Fig. 1. This produces a 2D image which has a *bas relief* appearance, as shown in Fig. 2(a). Specimen features (in this case, a few metaphase chromosomes from an orchid root tip preparation) appear with highlights and shadows at the edges, against a grey background. This provides a boost in high spatial frequency response (Cogswell & Sheppard, 1992), together with increased contrast for human viewing of 2D images. Meanwhile, axial resolution is increased, with optical sectioning occurring for high spatial frequency features in the specimen. However, unlike confocal fluorescence, this optical sectioning does not apply to low spatial frequencies in DIC.

A common approach to computer display of 3D microscopy datasets of biological specimens is 3D volume visualization (Kriete, 1992; Chen *et al.*, 1995). For

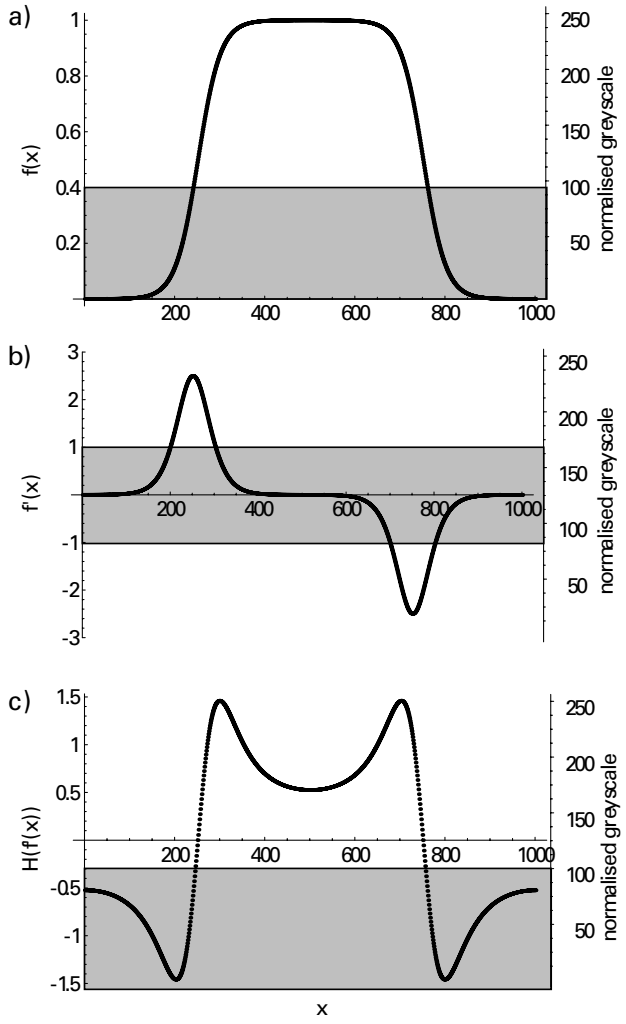

Fig. 1. One-dimensional model of a specimen feature. The shading specifies a range of intensities that are to be rendered transparent during volume visualization. A simple object is modelled in (a), with the shading showing how easily background signal can be selected to appear as transparent. Taking (a) to be a phase object, (b) shows the DIC case, where the best transparency range possible overlaps both the background and any details that may exist in the middle of the object, indicating that a more sophisticated transparency function is needed. The result of a Hilbert transform on the DIC signal is shown in (c), indicating that a background transparency threshold can now be set without obscuring details from the middle region of the object. In all cases the left vertical axis is in arbitrary mathematical units, and the right vertical axis is normalized for an eight-bit greyscale image.

fluorescence imaging, this relies on making the background transparent. This is easily done if the background is approximately black, indicating low fluorescence signal (see Fig. 1a). In the DIC case, the background is grey with small deviations in intensity. Making grey transparent in a 3D volume will reveal only the lateral shells of specimen features (Fig. 1b). Image processing techniques appropriate to gradient images need to be found and applied to DIC datasets before they can be displayed meaningfully in 3D.

Several authors have recently outlined methods that could be used to prepare DIC images for 3D visualization. Line integration and deconvolution (Kam, 1998) is an iterative method requiring calibration to the particular microscope in use. Variance filtering and directional integration using iterative energy minimization have also been proposed (Feineigle *et al.*, 1996). The rotational diversity technique (Preza *et al.*, 1998) combines numerous images taken of the specimen at different rotations. Direct deconvolution may be used, calibrated and optimized to reduce noise with a Weiner filter (van Munster *et al.*, 1997).

In this study we explore the suitability of the Hilbert transform for DIC image visualization. As a starting point we take the simple case of directional integration in 2D, as a method of retrieving the phase, given the phase gradient supplied by DIC. We then propose the 2D Hilbert transform as a qualitative alternative.

Image processing methods

Test specimen

In choosing a test specimen for studying DIC image processing methods, there is a balance between quantitative yet trivial specimens such as latex spheres, to complicated biological specimens which can best be appraised qualitatively, based on a knowledge of expected biological features. Particularly for segmentation of specimen features, the statistics and parameters used must be customised to the morphological characteristics of the class of specimens being examined. For this study, we chose to use plant chromosomes, as our emphasis is on creating qualitative techniques for visualization of cell morphology.

Integration

The obvious mathematical approach to recover a function from its gradient is integration. DIC effectively provides an optical differentiation. The DIC image is related to the phase gradient of the specimen, and the ability of the DIC system to resolve small differences in specimen phase is related to the amount of optical shear introduced by the DIC prism geometry (Pluta, 1989). In the imaging plane, the direction of differentiation is determined by the orientation of the Wollaston prism, and for DIC, this is often set at 45° to the lateral axes of the image. The first step in obtaining an accurate integration is to align the direction of shear or differentiation with one of the Cartesian axes of the digitized image. In our case, we have chosen to align the shear angle, and thus the direction of differentiation, to be parallel with the x axis of our image.

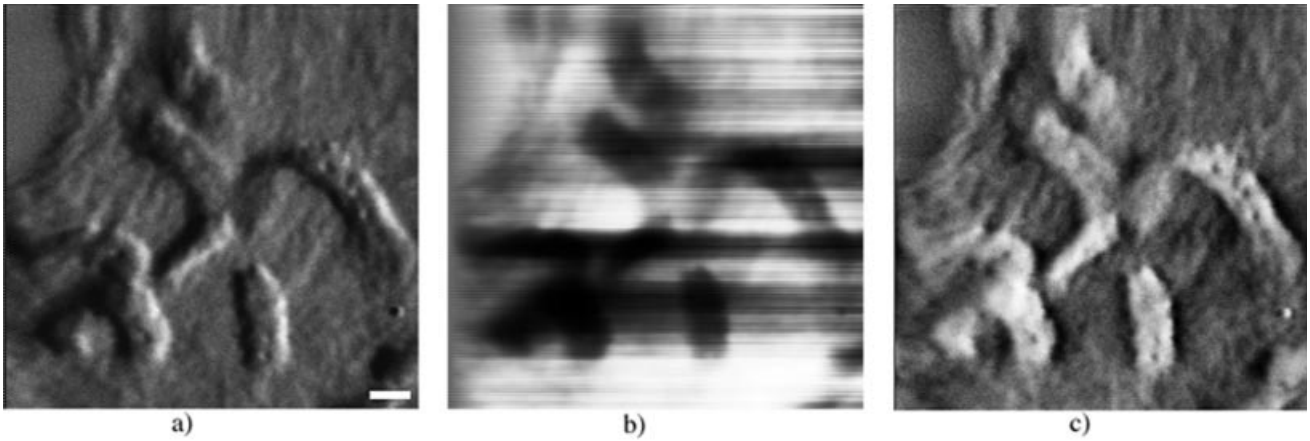

Fig. 2. Image processing of DIC images. (a) An unprocessed confocal transmission DIC image of metaphase chromosomes from an orchid root tip preparation illustrates the typical shading gradients that make standard feature extraction and 3D visualization techniques unusable. (b) The same image after line integration along the horizontal axis shows streaking due to the unknown constant of integration for each line. (c) The same image after applying a 2D Hilbert transform demonstrates that the chromosome features now could be isolated from the background using simple thresholding. Scale bar = 2 μm.

The integration may then be applied horizontally, line by line, to the digital image. Each line integrated will have an uncertainty from small errors in pixel values and an unknown constant of integration, which is lost by the differential imaging method. This constant will probably be different for each line, producing horizontal streaking in the image. In addition, integration acts as a low pass filter, suppressing high spatial frequency information in the image.

Hilbert transform

Turning to a spatial frequency analysis, a (real space) differentiation corresponds to a multiplication by the value of the spatial frequency parallel to the shear for each point in frequency space. Integration is then just the inverse, namely division by the spatial frequency. Both of these processes are antisymmetric (or odd) but the division selectively attenuates higher frequency components. What is needed is an antisymmetric transform or process that does not change the relative balance of the various frequency components. Such a transform exists and is known as the Hilbert transform (Bracewell, 1978; Oppenheim & Schafer, 1989). In 1D real space, the Hilbert transform *H(f(x))* is defined as

$$H\{f(x)\} = \hat{f}(x) = \frac{1}{\pi}\int_{-\infty}^{\infty} \frac{f(x')}{(x' - x)}\,\mathrm{d}x'. \qquad (1)$$

In Fourier space the apparent problems with the above singular integral disappear and the Hilbert transform results from a simple multiplication by a signum function:

$$F(s) = \int_{-\infty}^{\infty} f(s)\,\exp(-2\pi i s x)\mathrm{d}x, \qquad (2)$$

$$\hat{F}(s) = \int_{-\infty}^{\infty} \hat{f}(s)\,\exp(-2\pi i s x)\mathrm{d}x, \qquad (3)$$

$$\hat{F}(s) = i\,\mathrm{sgn}(s)F(s), \qquad (4)$$

where s is the spatial frequency, and $\mathrm{sgn}(s)$ is the signum function, which is equal to $+1$ for positive s and -1 for negative s.

In essence, the Hilbert transform keeps all the positive frequency components the same but reverses the sign of all the negative frequency components. Effectively, this makes the image features symmetric, removing the asymmetrical highlight and shading of objects. A simulation in one dimension is shown in Fig. 1(c). Note there is some ringing on either side of the peaks in the phase gradient. In fact the ringing is mainly due to the initial edge enhancement afforded by the derivative operation of the DIC optical system.

In two dimensions the Hilbert transform is not uniquely defined because the line between the positive and negative regions of the associated 2D signum function may have any orientation. In practice we choose the line orientation to be perpendicular to the DIC shear direction because it corresponds to the direction used by the integration method, and gives optimal results. The extension of the Hilbert transform into two dimensions is not well known in the area of digital image processing but it does occur frequently in the Fourier based analysis of 2D fringe patterns. An early use of what is essentially a 2D Hilbert transform occurs in Bone *et al.* (1986). In that instance the transform method was not actually called the Hilbert transform, but it can be shown to be essentially the same.

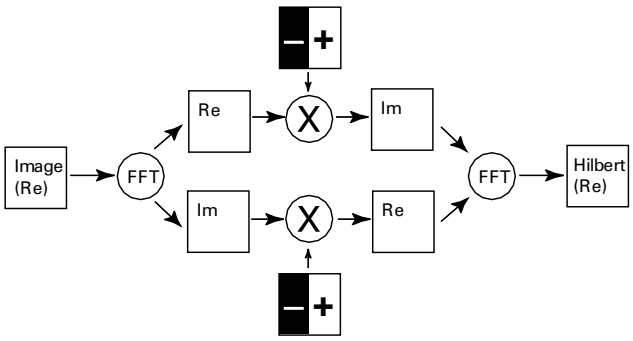

Fig. 3. Algorithm for the 2D Hilbert transform. This assumes the DIC shear angle is parallel with the x axis. 'Re' indicates the real part of the complex Fourier image, and 'Im' indicates the imaginary part. The middle step shows a multiplication of the real and imaginary parts by the Hilbert mask (a 2D step function).

The implementation of the 2D Hilbert transform for discretely sampled (image) data is shown schematically in Fig. 3. It is possible to implement an approximate Hilbert transform in real space using a convolution kernel (Oppenheim & Schafer, 1989; Chim & Kino, 1992) as implied by Eq. (1), but we chose the Fourier method implied by Eq. (4) for the images shown in this paper. An outline of the process (assuming the direction of differentiation is parallel to the x-axis) follows:

- fast Fourier transform (FFT) the image;
- multiply both the *real* and *imaginary* parts of the FFT by the Hilbert frequency response image (which consists of -1 for $y < 0$, 0 at $y = 0$, $+1$ for $y > 0$);
- swap the resultant real and imaginary parts;
- inverse FFT and take the real part as the new image (the imaginary part is essentially zero, if the Nyquist frequency components are correctly assigned, see for example Larkin *et al.*, 1997).

After applying the Hilbert transform to each 2D slice of our 3D datasets, we assembled 3D representations using volume rendering software, which in our case was VoxelView (Vital Images, Plymouth, Minnesota, U.S.A.).

Results and discussion

These image processing methods were applied to our DIC images, recorded in both confocal and conventional transmission, as part of our ongoing confocal transmission microscopy research. Theoretical investigations and experimental work by our group indicate that the imaging properties of confocal and conventional transmission DIC are similar in nature, but the confocal case indicates a possibility of increased axial resolution (Dixon & Cogswell, 1995), along with better contrast.

The results of our initial 2D line integration approach are shown in Fig. 2(b). There are two clear problems with this method. Firstly, the image shows unacceptable horizontal streaking. This may be attributed to the unknown constant of integration, which varies line by line. In addition, the image after integration is considerably blurred in contrast with the original, as is to be expected due to the low-pass filtering effect of integration.

The horizontal streaking problem may be dealt with by further developing directional integration in conjunction with an iterative energy minimization technique (Feineigle *et al.*, 1996). Alternatively, directional integration may be combined with iterative deconvolution (Kam, 1998). This last method requires calibration using a measurement of the shear produced by the DIC prism, and does not completely eliminate the streaks. Both methods produce the smoothing effect inherent to integration.

Applying a Hilbert transform gives a markedly improved result (Fig. 2c) compared with straightforward directional integration. The Hilbert transform produces a clear contrast between the features and the background. There is perhaps a slight ringing around the boundaries of the chromosomes (which is in agreement with the 1D simulation in Fig. 1). However, this is removed outside the boundaries for visualization using a transparency function modulated by intensity, as it is of lower intensity than the features. In our experience, the Hilbert transform has produced similar quality results across numerous DIC datasets.

The Hilbert transform may be compared with the variance (Feineigle *et al.*, 1996) in that it is a simple single pass computation that transforms the *bas relief* appearance into an intensity. However, the variance only highlights the *edges* of specimen features, whereas, within regions of higher phase, the Hilbert transform always has intensity levels higher than the background (see Fig. 1c). This makes the Hilbert transform more useful for 3D visualization than the variance.

Other more advanced techniques for reconstructing the phase from DIC images include Wiener filtered deconvolution (van Munster *et al.*, 1997) and rotational diversity (Preza *et al.*, 1998). Both these methods use quantitative models of the DIC imaging system in an effort to accurately restore the phase. Wiener filtered deconvolution requires a measurement of the DIC prism shear, and involves a trade-off between noise and high and low frequency components in the image. It also assumes there is no absorption in the specimen and that DIC has a linear response to phase in the specimen, which are generally not valid assumptions for complex biological objects at high numerical aperture. The rotational diversity technique involves taking multiple images of the specimen at differing rotations with respect to the DIC shear angle and then combining them using iterative optimization against the imaging model. This overcomes the loss of information for features perpendicular to the shear, a drawback to DIC imaging not addressed by other methods.

By contrast, the Hilbert transform is not necessarily a

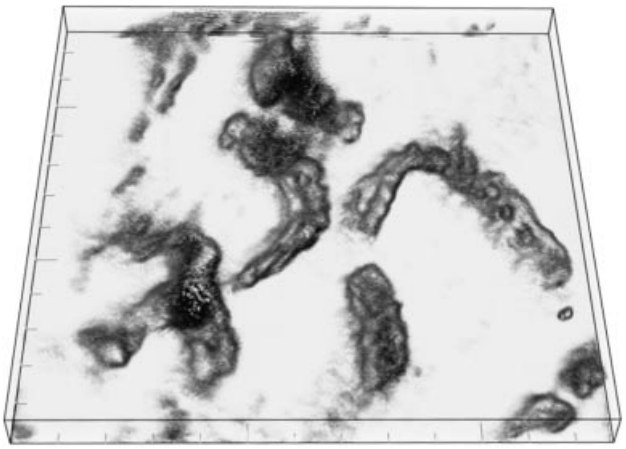

Fig. 4. A 3D visualization of a DIC through-focus series dataset (of which Fig. 2a is one optical section). A Hilbert transform was performed on each 2D slice in the stack. During visualization selective opacity was applied to voxels (3D pixels) according to their intensity. Horizontal scale is the same as Fig. 2, the volume height is 3.6 μm.

quantitatively accurate technique, such as integration or deconvolution might be. However, the images recorded using DIC are initially a mixture of non-linear phase and amplitude information. In these qualitative conditions it seems appropriate to use an image processing method that does not attenuate features of interest, namely high spatial frequency information and contrast of specimen objects from the background.

In terms of the technique itself, the Hilbert transform has the advantages that it requires no optical modification to the microscope, it is a simple single pass computation, and it does not require calibration for the shear of the DIC prism.

3D visualization

The Hilbert transform may be applied in turn to each 2D slice of a 3D dataset. A visualization of one such dataset is shown in Fig. 4, produced using the Hilbert transform and selective opacity based on intensity. The 3D images are from a focus series of orchid root tip metaphase chromosomes (of which Fig. 2a is one optical section). Comparison between 2D slices and the 3D visualization indicates that subtle structure available in the dataset is being borne out by the visualization. In particular, changes in phase along the z axis are clearly resolved. This fine detail was validated as being accurate by comparison with the features appearing in different z planes within the original 2D image slices (Fig. 5). This is especially evident when the dataset is rotated in an animation.

Conclusion

We have demonstrated that the Hilbert transform is a useful qualitative technique for effective 3D visualization of transmission DIC datasets. It overcomes the problems of streaking and high spatial frequency loss that occur in line-by-line integration techniques and it can be used for images of complex biological specimens that contain both phase and amplitude information. Because of its simplicity, the Hilbert transform technique can rapidly be applied to DIC datasets comprised of multiple focus planes using batched post-processing. This holds promise for future applications for 3D visualization of live-cell processes over time.

Acknowledgements

The authors would like to thank D. E. Wimber for providing the chromosome preparations used in this study. This research was supported by a grant of the Australian Research Council. Visualizations were generated using the Sydney Regional Visualization Laboratory (which is supported by the Australian Research Council) and the Australian Key Centre for Microscopy and Microanalysis.

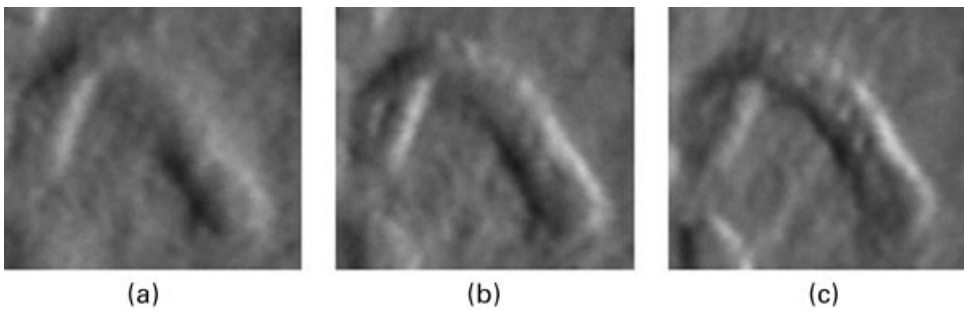

Fig. 5. Selected unprocessed 2D slices from the 3D dataset used in Fig. 4, cropped to highlight features that change through focus that are also clearly visible in the 3D visualization. This demonstrates that these fine details are preserved in the visualization. The three slices shown are at focal depths of 0.6 μm, 1.2 μm and 1.8 μm. The corresponding chromosome in Fig. 4 is in the middle right of the image.

References

Bone, D.J., Bachor, H.-A. & Sandeman, R.J. (1986) Fringe-pattern analysis using a 2-D Fourier transform. *Appl. Optics*, **25**, 1653–1660.

Bracewell, R.N. (1978) *The Fourier Transform and its Applications.* 2nd edn. McGraw-Hill, New York. p. 444.

Chen, H., Swedlow, J.R., Grote, M., Sedat, J.W. & Agard, D.A. (1995) The collection, processing, and display of digital three-dimensional images of biological specimens. *Handbook of Biological Confocal Microscopy (*ed. by J. B. Pawley), pp. 197–210. Plenum Press, New York.

Chim, S.S.C. & Kino, G.S. (1992) Three-dimensional image realization in interference microscopy. *Appl. Optics*, **31**, 2550–2553.

Cogswell, C.J. & Sheppard, C.J.R. (1992) Confocal differential interference contrast (DIC) microscopy: including a theoretical analysis of conventional and confocal DIC imaging. *J. Microsc.* **165**, 81–101.

Cole, R.W., Khodjakov, A., Wright, W.H. & Rieder, C.L. (1995) A differential interference contrast-based light microscopic system for laser microsurgery and optical trapping of selected chromosomes during mitosis *in vivo*. *J. Microsc. Soc. Am.* **1**, 203–215.

Dixon, A.E. & Cogswell, C.J. (1995) Confocal microscopy with transmitted light. *Handbook of Biological Confocal Microscopy* (ed. by J. B. Pawley), pp. 479–490. Plenum Press, New York.

Feineigle, P.A., Witkin, A.P. & Stonick, V.L. (1996) Processing of 3D DIC microscopy images for data visualisation, *Proc. IEEE Int. Conf. Acoustics, Speech, and Signal Processing*, 4, 2160–2163. IEEE, New York.

Hepler, P.K. & Gunning, B.E.S. (1998) Confocal fluorescence microscopy of plant cells. *Protoplasma*, **201**, 121–157.

Kam, Z. (1998) Microscopic differential interference contrast image processing by line integration (LID) and deconvolution. *Bioimaging*, **6**, 166–176.

Kriete, A., ed. (1992). *Visualization in Biomedical Microscopies: 3-D Imaging and Computer Applications.* VCH, Weinheim.

Larkin, K.G., Oldfield, M.A. & Klemm, H.U. (1997) Fast Fourier method for the accurate rotation of sampled images. *Optics Commun.* **139**, 99–106.

Oppenheim, A. & Schafer, R. (1989). *Discrete-Time Signal Processing.* Prentice Hall, New Jersey.

Pluta, M. (1989). *Advanced Light Microscopy: Specialised Methods.* Elsevier, Amsterdam.

Preza, C., Munster, E.B.V., Aten, J.A., Snyder, D.L. & Rosenberger, F.U. (1998) Determination of direction-independent optical pathlength distribution of cells using rotational-diversity transmitted-light differential interference contrast (DIC) images, *Three-dimensional and Multidimensional Microscopy. Image Acquisition and Processing V*, 3261, 60–70. SPIE, San Jose, CA.

Terasaki, M. & Dailey, M.E. (1995) Confocal microscopy of living cells. *Handbook of Biological Confocal Microscopy* (ed. by J. B. Pawley), pp. 327–346. Plenum, New York.

van Munster, E.B., van Vliet, L.J. & Aten, J.A. (1997) Reconstruction of optical pathlength distributions from images obtained by a wide-field differential interference contrast microscope. *J. Microsc.* **188**, 149–157.